Journal of the Brazilian Society of Mechanical Sciences and Engineering (2026) 48:614
https://doi.org/10.1007/s40430-026-06590-5

TECHNICAL PAPER

A numerical study comparing hydrodynamic performance of circular and square cross-sectional wetted venturi scrubbers

Furkan Turkoglu[1] · **Seyfettin Bayraktar**[2]

Received: 21 August 2024 / Accepted: 10 May 2026
© The Author(s) 2026

Abstract

The contaminants are cleared from the gas before they are released into the environment by venturi scrubbers that are easy to use and effective gas cleaning equipment. Venturi scrubbers use liquids to remove contaminants from the gaseous medium. In the present study, single and double-phase flows in both circular and square cross-sectional wetted venturi scrubbers are investigated by employing the computational fluid dynamics method. Air is sent to the venturi while water is injected from four circular circumferentially located nozzles. Simulations are performed for various water flow rates and air inlet velocities employing the Euler-Lagrangian-based Discrete Phase Model (DPM). The hydrodynamic performances of both types of scrubbers are compared to each other for various water flow rates, air inlet velocities and the liquid-to-gas (L/G) ratios. For the single-phase flow, it is seen that at the same air inlet velocity, the circular scrubber experiences a greater pressure reduction. For the double-phase flow, the pressure drop increases almost linearly with gas inlet velocity and water mass flow rate. As the liquid/gas (L/G) ratio increases, the pressure drop becomes significantly larger. The square cross-sectional scrubber yields the maximum collecting efficiency, approaching 96%, whereas the predicted effectiveness of the circular one is 58% at the lowest mass flow rate. It is also discovered that increasing the water flow rate and the inlet gas velocity decreases the collection efficiency in square scrubbers by 21% and in circular scrubbers by 24%.

Keywords Venturi · Scrubber · Gas-cleaning · Computational fluid dynamics (CFD) · Separation

List of symbols

CFD	Computational fluid dynamics
C_D	Drag coefficient
C_{vm}	Virtual mass coefficient
d	Diameter of the throat
d_p	Particle diameter
D	Diameter of the inlet and outlet sections
DPM	Discrete phase model
F_d	Force exerted by the discrete phase on the continuous phase
g	Gravitational acceleration
G_k	Generation of the turbulence kinetic energy due to the mean velocity gradient
I	Identity matrix
L/G	Liquid-to-gas ratio
m	Mass of the particle
S	Modulus of the mean rate-of-strain tensor
VOF	Volume of fluid
V_p	Particle volume
x_p	Particle position
Y_k	Dissipation of turbulence kinetic energy due to turbulence
Y_ω	Dissipation of the specific dissipation rate due to turbulence
2D	Two-dimensional
3D	Three-dimensional

Greek symbols

α	Enlargement angle of the diverging section
β	Contraction angle of the convergent section
ρ	Fluid density
u	Fluid velocity

Technical Editor: Gilmar Mompean.

✉ Seyfettin Bayraktar
sbay@yildiz.edu.tr

[1] Department of Naval Architecture and Marine Engineering, Yildiz Technical University, 34349 Istanbul, Turkey

[2] Department of Marine Engineering, Yildiz Technical University, 34349 Istanbul, Turkey

Published online: 04 August 2026

p	Fluid pressure
τ	Stress tensor
μ	Dynamic viscosity of the fluid
σ_k	Turbulent Prandtl numbers for k
σ_ω	Turbulent Prandtl numbers for ω

1 Introduction

The scrubbers are pollution control devices used to separate unwanted pollutants from an industrial waste gas stream before releasing it into the atmosphere. Basically, two kinds of scrubbers, known as dry and wet scrubbers, are in use today. Dry scrubbers utilize dry reaction materials such as alkaline slurry, while wet scrubbers use liquids such as water to clean the contaminated gases. Among many types of wet scrubbers such as chemical/gas, ammonia, chloride and sulfuric acid scrubbers the particulate/venturi scrubbers are distinguished from the other types due to their high collection effectiveness [7, 39] and hence they are used as the main components of filtered vented containment systems [6], dust removers that are suitable for underground mine [25], desulphurisation tools of cement flue gases [41], and disposals of exhaust gas emission from operating ships [44, 45]. Based on the scrubbing liquid supplied at the throat through a nozzle, the venturi scrubbers can be divided into two fundamental types: forced feed injection and self-priming venturi scrubbers [28]. In the first kind, an external device, such as a pump, causes the liquid to flow into the throat,in the self-priming type, however, the fluid enters the venturi scrubber as a result of the difference in pressure between the tank's hydrostatic head and the throat's static pressure Lehner et al., [28].

Using both the numerical and experimental techniques various parameters affect the performance of the venturi scrubbers such as the liquid-to-gas (L/G) ratio [8, 17], droplet size distribution (Talaie et al., [43]), turbulence intensity, penetration of the liquid jet [4, 21], and the geometrical arrangement of the scrubber, including the length and diameter of the throat [2, 3], quantity and placement of its liquid injection nozzles [20], etc. have been investigated so far. The majority of experimental studies were done with laboratory-scale scrubbers. For example, [18] used a rectangular cross-section venturi scrubber and proposed a new correlation that can predict the separation efficiency quite accurately. Employing a self-priming venturi scrubber, Zhou et al. [53] reported that increasing both the gas velocity and the injection flow rate enhances its performance. The study showed that gas velocity significantly affects efficiency, especially at low injection rates. A longer throat and smaller diffuser angle enhance retention performance for small-sized aerosols. The entry and exit angles of venturi nozzles were also studied by [27]. It was shown that the pressure drop impacts the exit angle and that, except for 30 degrees, the bubble size decreases as the angle increases. After a series of experiments, [1] concluded that there are optimum values for both gas and liquid flow rates for the efficient operation of the scrubber. Beyond the optimum values, efficiency may decrease due to bad coverage at the throat and less contact between the liquid and gas. It was observed that the jet penetration length increases with higher gas flow rates but decreases with lower flow rates. With the rapid advancement of computer technology and numerical methodologies, computational fluid dynamics (CFD) investigations have become an important and reliable tool in engineering research, and scrubbers are no exception [46]. Utilizing the Eulerian–Lagrangian method Pak and Chang [33] revealed that both the collection efficiency and pressure loss increase with increasing the L/G ratio in a circular venturi scrubber, as reported previously by [22]. [37] employed a population balance equation in conjunction with an Eulerian–Eulerian three-dimensional (3D) numerical model to focus on the pressure decrease in a rectangular cross-section scrubber. The employed k-epsilon turbulence model successfully predicted the pressure drop for the air–water system and was used to study the effect of configuration and diameter of the nozzles on the pressure drop as neither the configuration nor the diameter have impact on the pressure drop. The prediction performance of a commercially available software, Ansys Fluent and an open-source code OpenFoam was evaluated by Attaullah, Niazi et al., [10] for a 3D circular venturi scrubber. It was seen that, for the gas velocity of 50 m/s at the throat section, as the L/G ratio increases the numerical results obtained from Fluent start to deviate from the experimental data. For $0 < L/G < 1$ both OpenFoam and Fluent predict almost the same pressure drop. Using the models proposed by [15] and [31] they shown that the relative error in the calculation of collection efficiency by Mohebbi model is less compared to the Calvert model.

It is commonly accepted that the pressure drop is the most crucial factor in the design and operation stages of venturi scrubbers, hence, much efforts have been devoted to the prediction of pressure drop in the venturi scrubbers. Although it is possible to obtain how pressure drop changes with other parameters by means of experimental and numerical methods, it is also possible to calculate the pressure drop utilizing some analytical models. Goncalvez et al., [19] summarized and compared the pressure drop found by means of such models with the experimental data for a wide range of throat diameter changing from 19 to 160 mm. Analytical models of [11, 14, 16, 23, 24, 29, 48, 52] were selected for comparison and it was highlighted that particular consideration needs to be given to the assumptions of each model and operating conditions of the experimental studies used

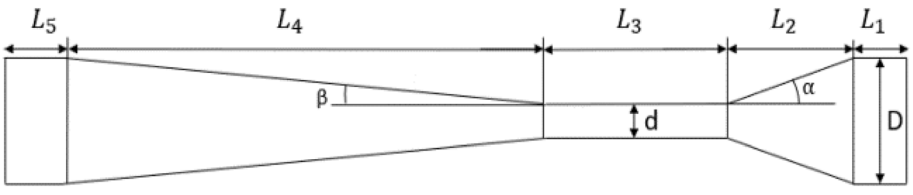

Fig. 1 Dimensions of the venturi scrubbers

Design	D (mm)	d (mm)	L_1 (mm)	L_2 (mm)	L_3 (mm)	L_4 (mm)	L_5 (mm)	α (°)	β (°)
Circular	250	122.5	230	240	300	740	60	17	5
Square	250	122.5	230	240	300	740	60	17	5

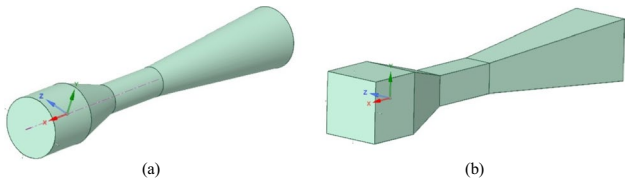

Fig. 2 Designed circular (**a**) and square (**b**) cross-sectional scrubbers

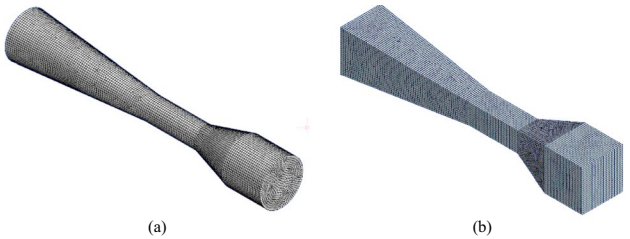

Fig. 3 Mesh structure for **a** circular and **b** square cross-sectional scrubber without nozzles

for comparisons. It can be concluded that researchers must be cautious when validating their experimental or numerical data with these analytical models. Pressure drop in a large-scale circular venturi scrubber was measured, and the impact of gas velocity and liquid flow rate was examined for two different liquid injection methods-spray and film injection [39]. It was reported that the pressure drop is influenced by the droplet fraction, the liquid injection technique, and the rates of both the gas and liquid phases.

As highlighted in the cited references, the performance of wet venturi scrubbers with either circular or non-circular cross-sections has been extensively investigated individually because both geometries offer distinct advantages and disadvantages in the design and application. Due to their competing characteristics, there is a need for a careful choice of the appropriate geometry based on the requirements. Although much effort has been devoted to the circular or non-circular cross-section scrubbers in the related literature, no comprehensive investigation has been done on comparing their hydrodynamic performance under the same operating conditions. Therefore, the present study aims to close this gap by comparing key performance parameters such as velocity change, pressure drop, collection efficiency, the effect of the gas inlet velocity and liquid-to-gas (L/G) ratio when both scrubber designs have the same dimensions.

2 Computational details

This section presents the geometrical details of both circular and square cross-sectional venturi scrubbers such as dimensions, generated mesh structure and number of mesh elements, initial and boundary conditions and governing equations.

2.1 Geometry

The study examines scrubbers with dimensions identical to those reported by Silva [40]. The square cross-sectional scrubber was developed by modifying the circular cross-sectional configuration described by [40], while maintaining a constant hydraulic diameter. The dimensions of both scrubbers are shown in Fig. 1, where L_1 (230 mm), L_2 (240 mm), L_3 (300 mm), L_4 (740 mm) and L_5 (60 mm) denote the length of the inlet, converge, throat, diverge (also called diffuser) and outlet sections, respectively.

The hydraulic diameters at the inlet, throat, and outlet sections are the same for both designs (d = 122.5 mm, D = 250 mm). The working liquid, water, is injected from four evenly distributed circular nozzles with a diameter of $d_{nozzle} = 1.5$ mm that are located just before the converging sections [47]. The circular and square cross-sectional scrubbers, as well as the Cartesian coordinate system, are given in Fig. 2.

2.2 Mesh structure

The scrubber, considered as the computational domain, was divided into smaller volumes known as a grid or mesh to compute the flow variables. As shown in Fig. 3, smaller mesh elements are used to capture the velocity gradients in the throat and intersection regions. A non-homogeneous mesh structure consisting of hexahedral elements is employed. For clarity, the number of mesh elements shown has been reduced.

Before the parametric analysis, a mesh independence study was carried out to guarantee that the simulation results are mesh independent. Using a circular cross-section venturi five different meshes, referred to as M1–M5, were generated

Table 1 Mesh independence study

Mesh title	Number of mesh elements	Minimum element size	Trapped/injected droplets	Collection efficiency (%)	Change in efficiency (%)
M1	152,550	20	101/251	40	–
M2	183,000	10	109/251	43	+7.5
M3	210,219	8	114/251	45	+4.6
M4	285,473	6	113/251	45	–
M5	353,247	5	113/251	45	–

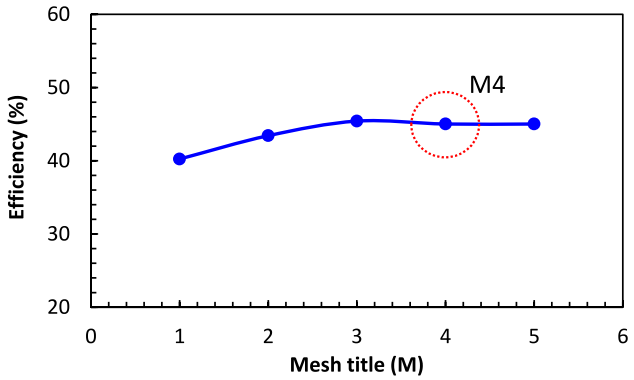

Fig. 4 Mesh independence study and the selected mesh (M4) for the next analyses

for this purpose. Table 1 displays the number of mesh elements, the minimum element size, the ratio of trapped to injected droplets, and accordingly, the collection efficiency of the scrubber, which is explained in detail later.

To visualize how changing the number of mesh elements affects the collection efficiency, the data given in Table 1 is plotted in Fig. 4. For the subsequent simulations, M4 is selected because the collection efficiency remains the same when the number of mesh elements increases from M3 to M4.

2.3 Governing equations

The CFD method is extensively utilized in research across various scientific and engineering disciplines to analyze system performance [32, 38, 50]. Among the leading CFD tools, Ansys Fluent, which employs the finite volume method to investigate different types of complex flows, including multiphase flows is used here. The present CFD study incorporates the Euler–Lagrange approach-based Lagrangian DPM, in which the fluid phase is treated as a continuum through the solution of the Navier–Stokes equations, and the dispersed phase is considered by following a large number of droplets through the computed flow field. The Eulerian–Lagrangian model requires fewer empirical equations and is more suited to give in-depth details on the discrete phase [30]. In the present study, it is preferred to measure collection efficiency. The continuity and momentum equations, as indicated below, are the governing equations for incompressible, Newtonian, isothermal, three-dimensional, and turbulent two-phase (air with liquid droplets) flow.

2.3.1 Continuous phase equations

The general governing equations for the continuous phase are the continuity (Eq. 1) and the momentum equations (Eq. 2) [51].

$$\frac{\partial \rho}{\partial t} + \nabla (\rho u) = 0 \tag{1}$$

$$\frac{\partial (\rho u)}{\partial t} + \nabla (uu) = -\nabla p + \nabla \tau + \rho g + F_d \tag{2}$$

where ρ and u show density and velocity of the continuous phase, p stands for the static pressure and F_d is the drag force. The stress tensor (τ) is given in detail in Eq. 3.

$$\tau = \mu \left(\nabla u + \nabla u^T \right) - \frac{2}{3} \mu (\nabla u) I \tag{3}$$

Here, μ, ∇u and ∇u^T are the dynamic viscosity of the fluid, gradient of the velocity vector and transpose of the velocity gradient tensor that implies symmetric velocity changes, respectively.

2.3.2 Discrete phase model (DPM) equations

The equations of motion in the Lagrangian framework are solved to monitor the discrete phase droplets. By integrating the equations of motion for each particle, the trajectory and properties of each one are calculated while considering the various forces acting on them. The governing equations for DPM are the particle motion (Eq. 4) and the total forces on the particle such as the drag (Eq. 5), gravity (Eq. 6), buoyancy (Eq. 7), virtual mass force (Eq. 8) and kinematic relationship between the position and velocity of the droplet (Eq. 9). It should be noted that each equation is the single differential equation characterizes the droplets individually according to DPM.

$$\frac{\mathrm{d}u_p}{\mathrm{d}t} = \frac{F}{m_p} \tag{4}$$

$$F_d = \frac{1}{2} C_D \rho \frac{\Pi d_p^2}{4} |u - u_p| (u - u_p) \tag{5}$$

$$F_g = m_p g \tag{6}$$

$$F_b = -v_p \rho g \tag{7}$$

$$F_{v_m} = 0.5 m_p \frac{\rho}{\rho_p} \left(u_p \nabla \mathrm{u} - \frac{\mathrm{d}u_p}{\mathrm{d}t} \right) \tag{8}$$

$$\frac{\mathrm{d}x_P}{\mathrm{d}t} = u_p \tag{9}$$

Various turbulence models such as Standard k-epsilon [37], Realizable k-epsilon [2, 3], RNG k-epsilon [13], Reynolds Stress Turbulence Model [49] and SST k-epsilon turbulence model [35] were used for flow in venturi scrubbers that implies that there is no consensus on the selection of the turbulence model. In the present study, the SST k-omega turbulence model is selected due to its advantages over the mentioned turbulence models [42]. Firstly, it blends the k-omega model near walls and the k-ε model in the far field, which provides a more accurate representation of the near-wall region, which is critical for flows in venturi scrubbers due to the high-velocity gradients and complex interactions between the liquid and gas phases. Secondly, it is well-suited for adverse pressure gradients, which are common in venturi scrubbers. It accurately predicts flow separation and reattachment. It is also less sensitive to the specification of inlet turbulence levels. Finally, compared to the Reynolds Stress Turbulence Model (RSM), the SST model often offers a better balance between accuracy and computational cost.

The governing equations for the SST k-omega turbulence model are the transport equations of the turbulence kinetic energy (Eq. 10) and its dissipation rate (Eq. 11). The SST k-omega model uses a modified turbulent viscosity formulation to account for the transport effects of the turbulent shear stress.

$$\begin{aligned} \frac{\partial}{\partial t}(\rho k) + \frac{\partial}{\partial x_i}(\rho k u_i) = \frac{\partial}{\partial x_j}\left(\left(\mu + \frac{\alpha^* \rho \frac{k}{\omega}}{\sigma_k}\right)\frac{\partial k}{\partial x_j}\right) \\ + \left(-\rho \overline{u_i' u_j'} \frac{\partial u_j}{\partial x_j}\right) - Y_k \end{aligned} \tag{10}$$

$$\begin{aligned} \frac{\partial}{\partial t}(\rho \omega) + \frac{\partial}{\partial x_i}(\rho \omega u_i) = \frac{\partial}{\partial x_j}\left(\left(\mu + \frac{\alpha^* \rho \frac{k}{\omega}}{\sigma_\omega}\right)\frac{\partial \omega}{\partial x_j}\right) \\ + \left(\frac{\omega}{k} G_k\right) - Y_\omega \end{aligned} \tag{11}$$

where α^* is the coefficient that damps the turbulent viscosity causing a low-Reynolds number correction. To evaluate the generation of turbulence kinetic energy G_k in a manner consistent with the Boussinesq hypothesis;

$$G_k = \mu_t (S_{ij} S_{ij}) \tag{12}$$

The instantaneous gas velocity of the continuous phase is predicted by discrete ndom walk model. The coupling of pressure and velocity is required for DPM. Second-order discretization of space is specified for pressure, momentum, turbulent kinetic energy, and its dissipation rate. The collection efficiency was calculated as follows.

$$Collection\, efficiency\, (\eta) = \frac{Trapped\, droplets}{Total\, droplets} \tag{13}$$

2.4 Boundary conditions

The present study evaluates water and air flow through both types of scrubbers under varying water flow rates and air inlet velocities, as shown in Table 2. Two geometries (circular and square), five different water mass flow rates (0.001, 0.005, 0.019, 0.038, and 0.075 kg/s) and four different air velocities (5, 10, 15, and 20 m/s), resulting in a total of 40 different scenarios, are studied.

At the inlet section of the scrubber, a velocity inlet condition was defined, while the mass flow rate was specified at the inlets of the nozzles where water is sprayed. The outlet of the scrubber was set to pressure outlet. The other boundary conditions used in the study are turbulence intensity and turbulence characteristic length. Depending upon the inlet air velocity, the various turbulence intensities in the range of 3.6% and 3.8% are specified, while the turbulence characteristic length is calculated as 0.0185 m using $l = 0.07 D_h$ formula [9].

3 Main findings and discussion

3.1 Validation studies

Validation of the present study is performed by comparing the present results with the experimental data of [40] and the numerical output of [26] for the same dimensions and operating conditions as described in their studies. Comparisons for single- and double-phase flows with a water mass flow rate of 0.02 kg/s and the throat velocities of 34 m/s and 70 m/s are shown in Fig. 5. Similarly, the change in axial velocity component obtained experimentally by [40] is shown in Fig. 6 for single and double phase flows. As shown in Fig. 5a, both the experimental data of [40] and the present study show similar trends except for a slight deviation, particularly after the converging section where the

Table 2 Investigated cases in the study

Geometry	Case	Scrubber geometry	Water flow rate (kg/s)	Air velocity (m/s)	Geometry	Case	Scrubber geometry	Water flow rate (kg/s)	Air velocity (m/s)
Circular (C)	C1	Circular	0.001	5	Square (S)	S1	Square	0.001	5
	C2	Circular	0.005			S2	Square	0.005	
	C3	Circular	0.019			S3	Square	0.019	
	C4	Circular	0.038			S4	Square	0.038	
	C5	Circular	0.075			S5	Square	0.075	
	C6	Circular	0.001	10		S6	Square	0.001	10
	C7	Circular	0.005			S7	Square	0.005	
	C8	Circular	0.019			S8	Square	0.019	
	C9	Circular	0.038			S9	Square	0.038	
	C10	Circular	0.075			S10	Square	0.075	
	C11	Circular	0.001	15		S11	Square	0.001	15
	C12	Circular	0.005			S12	Square	0.005	
	C13	Circular	0.019			S13	Square	0.019	
	C14	Circular	0.038			S14	Square	0.038	
	C15	Circular	0.075			S15	Square	0.075	
	C16	Circular	0.001	20		S16	Square	0.001	20
	C17	Circular	0.005			S17	Square	0.005	
	C18	Circular	0.019			S18	Square	0.019	
	C19	Circular	0.038			S19	Square	0.038	
	C20	Circular	0.075			S20	Square	0.075	

present study predicts slightly higher velocity at the throat for the single-phase flow. In the case of double phase flow, the agreement between the two studies is better although slightly lower velocities are predicted by the present study. The deviation between the experimental data of [40] and the present study is more evident in Fig. 5b for lower double-phase flow velocity at the throat, possibly due to the numerical methods employed in the present CFD model. However, the difference between the two studies does not exceed 8% for double-phase flow at the throat.

The comparison with the results of [26] introduced in Fig. 6a shows that both studies are largely consistent, with only small differences in the converging section until the throat section. However, for the double phase flow, some differences, particularly in the throat and after throat regions, are identified where the present study predicts a lower velocity. Regarding Fig. 6b, it is seen that both curves exhibit the same overall trend of a pressure drop, reaching a minimum at the throat, followed by a pressure recovery downstream. Related to the velocity distribution introduced in Fig. 6a, due to the increase in the velocity at the throat, where the cross-sectional area is the smallest, the pressure drops in the converging section and then increases as the area increases, causing the pressure to recover after the throat. The close match between the present study and the numerical output of [26] confirms once again the accuracy and reliability of the present study in predicting both velocity and pressure distributions for single-phase and double-phase flows in scrubbers, although there are slight deviances, which are possibly due to turbulence and/or phase interaction modeling.

3.2 Parametric studies

This section introduces the velocity and pressure distributions for both single-phase and double-phase flows in circular and square cross-sectional wet scrubbers of identical dimensions and operating conditions. Additionally, key parameters such as pressure drop, liquid-to-gas (L/G) ratio, and collection efficiency for various water flow rates and gas inlet velocities are compared for both types of scrubbers, highlighting their hydrodynamic performance.

3.2.1 Single-phase flow

The present study begins with single-phase flow simulations, then proceeds to two-phase flow to examine how nozzle-injected water influences the global characteristics. Figure 7 depicts how velocity changes along the circular and square cross-sectional venturi scrubbers at two different inlet gas velocities (5 m/s and 10 m/s) at single-phase flow. It is seen that regardless of the geometry, the flow accelerates immediately toward the converging section of the scrubber and reaches its maximum at the throat due to the smallest cross-sectional area. Then, the flow decelerates downstream the throat as it enters the divergent section, where the influence

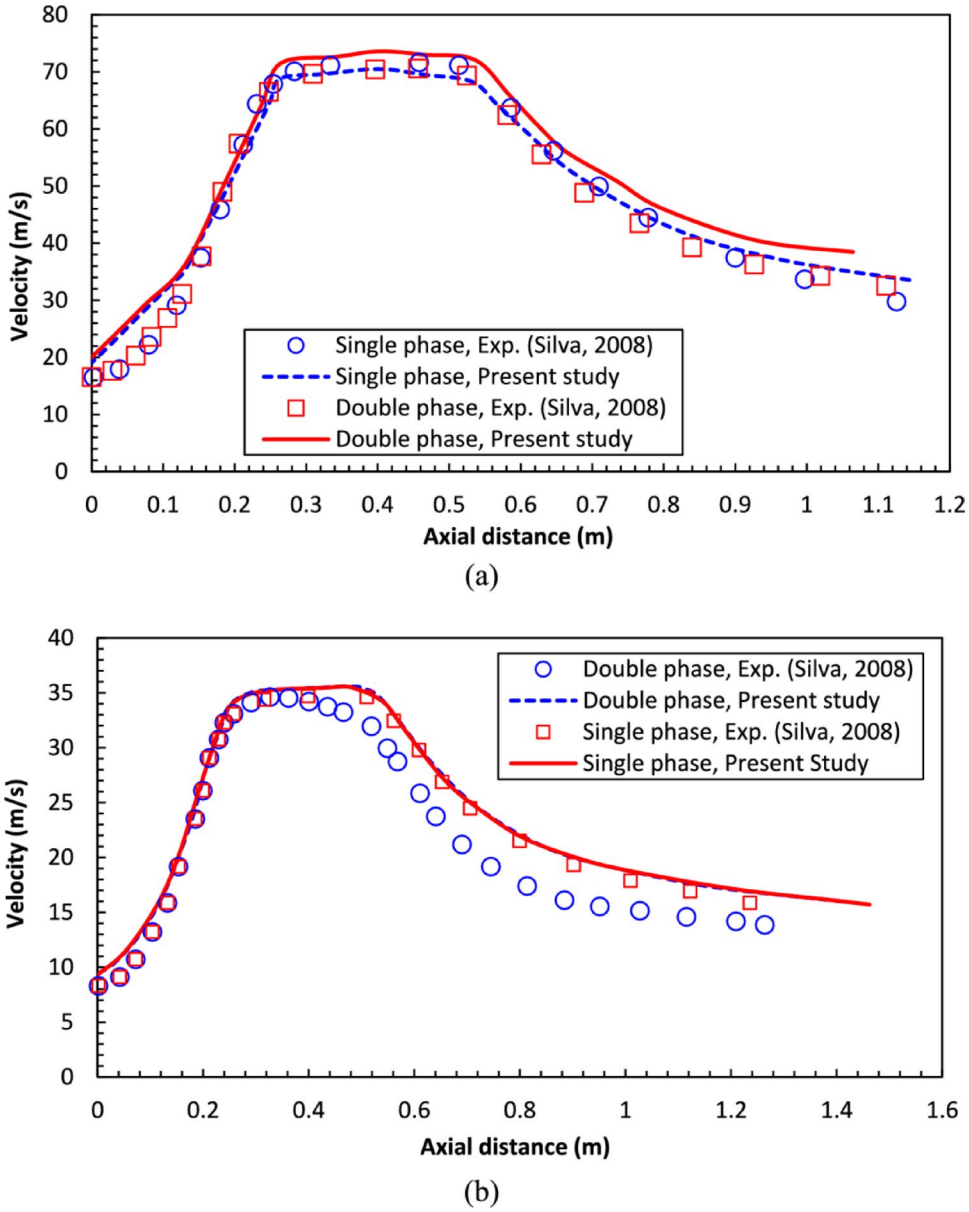

Fig. 5 Comparison of the present study with experimental data of [40] for single-phase flow at throat velocity of **a** 70 m/s and **b** 34 m/s and double-phase at water flow rate of 0.02 kg/s

of the shape of the scrubbers is observed. Here, due to keeping higher momentum arising from the existence of secondary flows and corner vortices that delay the flow separation, the square cross-section displays a somewhat flatter velocity decrease compared to the sharp velocity decay in the circular cross-sectional scrubber.

The pressure distributions for both geometries and inlet velocities are plotted in Fig. 8. A pronounced pressure drop is observed as the flow accelerates toward the throat region, followed by a gradual pressure recovery in the diffuser section. At both inlet velocities, the circular cross-sectional scrubber exhibits a larger pressure drop at the throat compared to the square scrubber. This difference becomes more evident at the higher velocity of 20 m/s. Although the axial velocity profiles presented in Fig. 7 show that both geometries reach similar peak velocity levels at the throat due to their close cross-sectional areas, the mechanical energy cost to achieve this acceleration differs. In the circular geometry, the flow transition is more streamlined, allowing for a more effective conversion of static pressure into kinetic energy with minimal interference. Conversely, in the square cross-sectional scrubber, the presence of flat walls and corner regions leads to the development of recirculation zones. These zones locally dissipate kinetic energy through turbulence, which acts to limit the effective acceleration of the core flow. Consequently, the square geometry maintains a higher static pressure at the throat and exhibits an earlier onset of pressure recovery compared to the circular configuration.

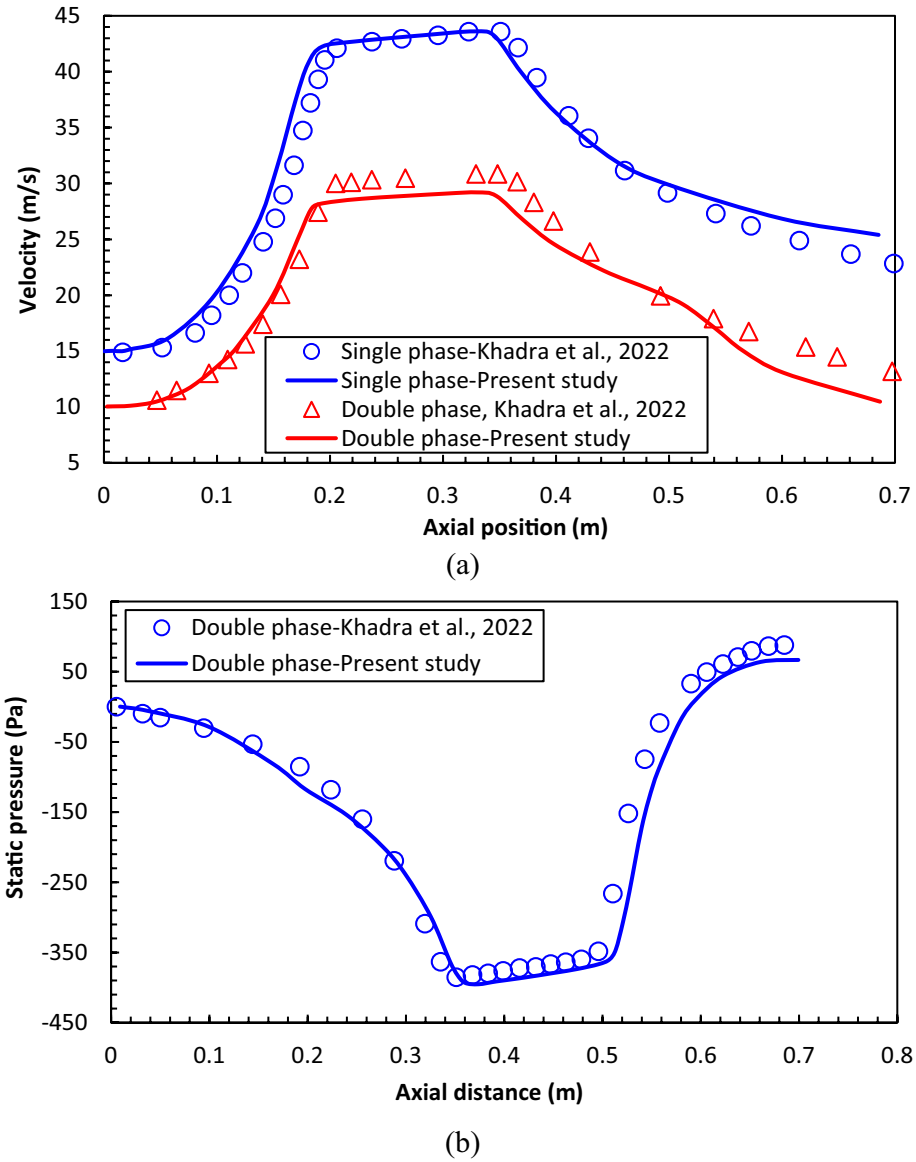

Fig. 6 Comparison of the present study with the numerical results of [26] for single-phase flow (V_{throat} = 10 m/s) and double-phase (V_{throat} = 15 m/s, m_{water} = 0.02 kg/s)

The single-phase velocity contours shown in Fig. 9 illustrate the influence of cross-sectional geometry on axial flow acceleration and recovery in the scrubbers at air inlet velocity of 20 m/s. For both configurations, the flow accelerates as it moves toward the throat, reaching maximum velocities due to the reduction in cross-sectional area, and subsequently decelerates in the downstream expansion. While both geometries show similar qualitative acceleration and deceleration trends, the circular scrubber provides a more symmetric axial velocity distribution, whereas the square cross-section introduces geometric effects that lead to broader high-velocity regions and enhanced transverse velocity non-uniformity.

3.2.2 Double-phase flow

In the double-phase flow, water is injected from four circular cross-section nozzles into the scrubber as air flows. Figure 10 compares the axial velocity profiles taken from the center of both circular and square cross-sectional geometries under double-phase flow. It is seen that the axial velocity increases as the flow moves toward the throat, forming a high-velocity core. With respect to the single-phase flow, the injection of water induces localized disturbances and enhances momentum exchange, resulting in a non-uniform axial velocity field that persists upstream of the throat and gradually relaxes further to the exit. The square cross-sectional scrubber causes the development of a broad region of nearly uniform axial velocity within the throat, characterized by a plateau-like distribution in the core flow that does

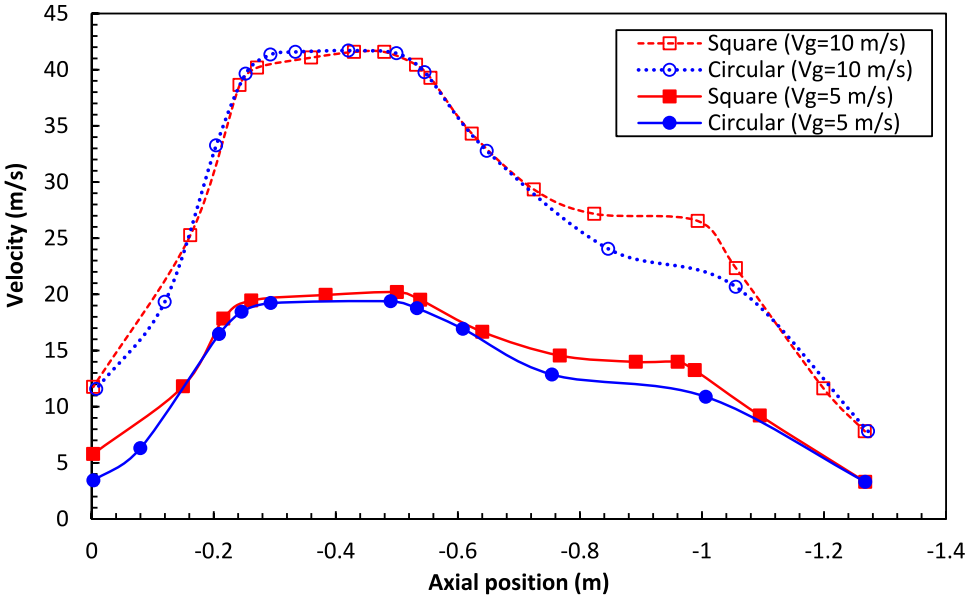

Fig. 7 Velocity profiles for circular and square cross-sectional venturi scrubbers for single-phase at V_g = 5 m/s and 10 m/s

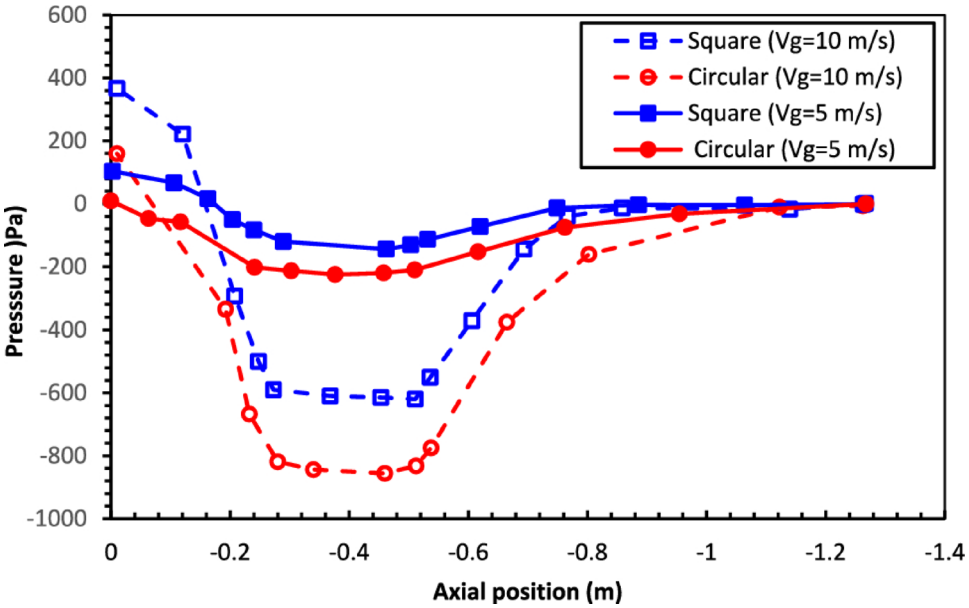

Fig. 8 Pressure changes in circular- and square-cross-section venturi scrubbers for single-phase at Vg = 5 m/s and 10 m/s

not appear in the circular configuration. This behavior indicates more effective distribution of axial momentum due to the combined effects of liquid injection and the presence of flat walls and corner regions in the square cross-section. As the flow continues downstream, the square geometry exhibits a smoother deceleration and recovery of axial velocity, with reduced peak values and weaker gradients compared to the circular scrubber. These results suggest that, the square cross-section promotes a more homogeneous axial velocity field, while the circular geometry favors stronger core acceleration and sharper velocity gradients.

3.2.2.1 Pressure drop The most important parameter in the scrubbers is the pressure drop because, according to the magnitude of the pressure drop at the throat section, the kinetic energy of the fluid passing through the throat increases and enables effective collection of the particles on the droplets potentially distributed in the gas stream (Ahmed et al., [5]; [36]). The plots presented in Fig. 11 show the pressure change along a circular and square scrubber for various water flow rates at air inlet velocity of 20 m/s. For both types of scrubbers, the pressure drop is highest at the greatest water flow rate and lowest at the minimal water flow rate. This is because there is more water in the scrubber, which creates more resistance to flow, leading to a higher pressure drop at the higher water flow rates. Similar to the

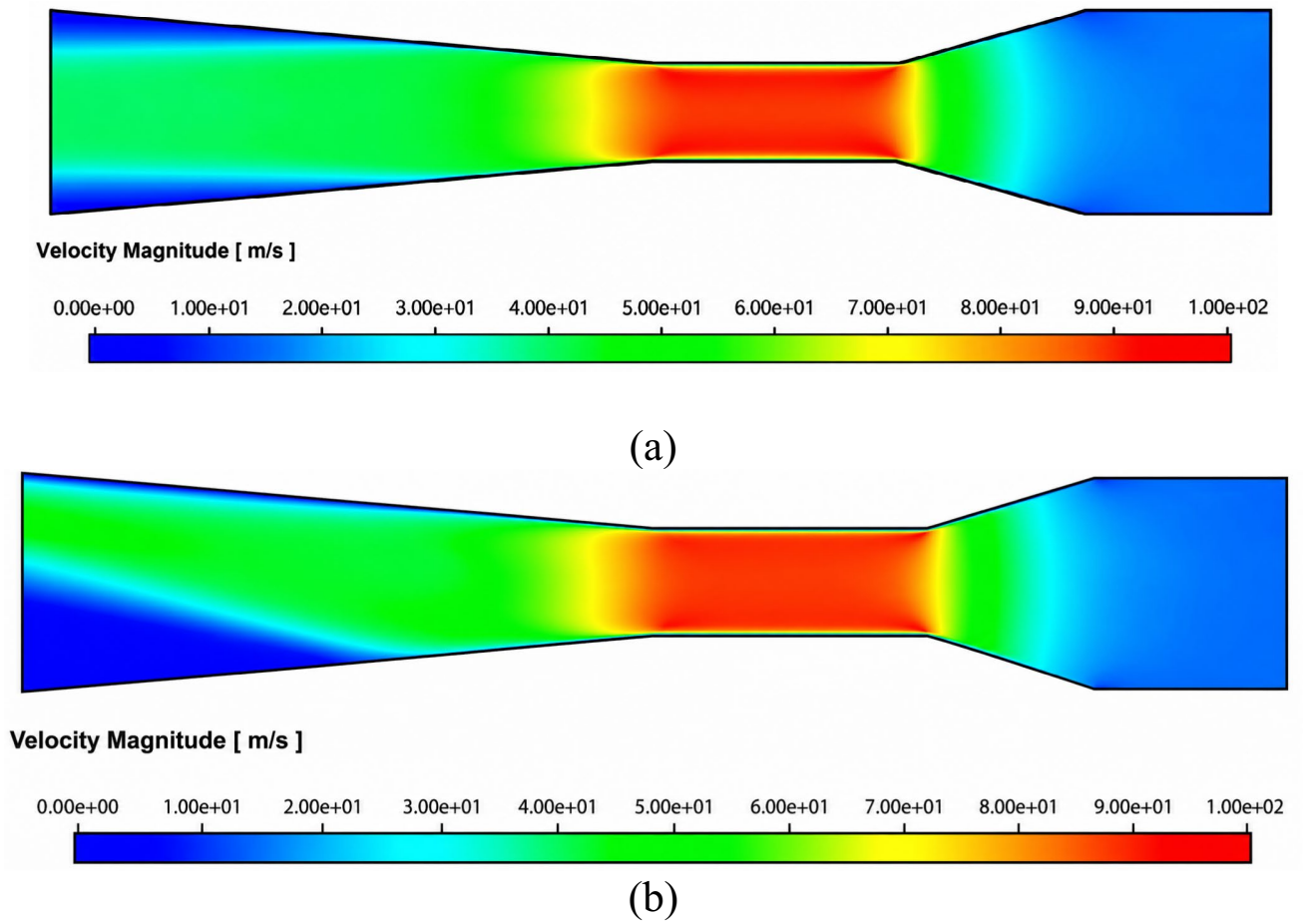

Fig. 9 The x-component velocity contours in the a) circular and b) square cross-sectional scrubbers at the inlet velocity of 20 m/s in single-phase flow

single-phase flow, in the two-phase flow, the lowest pressure occurs in the circular cross-sectional scrubber.

A slight oscillatory behavior is observed in the pressure distribution near the axial location $x \approx -0.5$ m, corresponding to the converging section upstream of the throat. This region is characterized by strong flow acceleration and steep pressure gradients. The oscillations are attributed to localized flow adjustments associated with the transition into the contraction, where boundary layer development and geometric curvature influence the pressure field. Additionally, a minor contribution from numerical discretization cannot be excluded, as such fluctuations are known to occur in regions with high gradients. A mesh sensitivity analysis indicated that the magnitude of these oscillations decreases with grid refinement, confirming that they are localized and do not impact the overall pressure trend or the conclusions drawn from the results.

Here, the pressure drop is quantified as the difference in area-weighted average static pressure between two cross-sections. For example, the analysis of flow acceleration toward the throat, the local pressure drop is defined relative to the inlet. Although not shown here, further studies revealed that, regardless of the scrubbers' cross-section, the pressure decreases more as the gas inlet velocity rises and becomes nearly independent of the water flow rate. The given plots in Fig. 12 show the relationship between gas inlet velocity and pressure drop for various configurations of scrubber geometry and water flow rates. Regardless of the cross-section geometry, the pressure drop increases with increasing both gas inlet velocity and water flow rate. Higher mass flow rate significantly increases the pressure drop, especially at higher velocity, indicating a higher resistance to flow as stated before. The circular cross-sectional venturi scrubber provides higher pressure drops than the square cross-section, no matter what the water flow rate is. This is due to differences in the flow dynamics and frictional losses associated with the geometry. At lower velocities (15–25 m/s), the pressure drops for all configurations are relatively close to each other, indicating that at low velocities, the effect of geometry and mass flow rate on pressure drop is less significant. This suggests that for applications

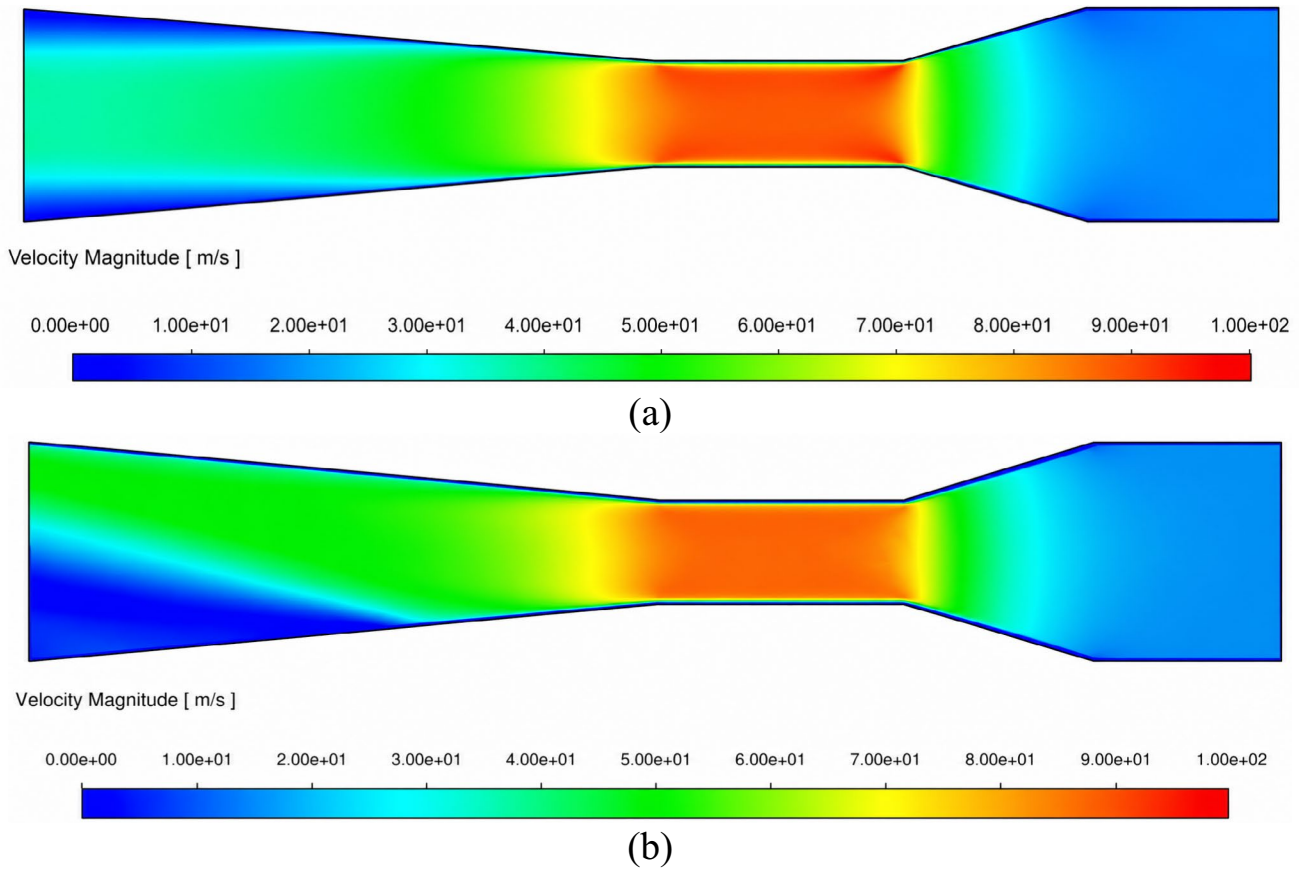

Fig. 10 The x-component of velocity contours in the a) circular and b) square cross-sectional scrubbers at the inlet velocity of $V_g = 20$ m/s for $m_w = 0.038$ kg/s (double phase)

operating at low gas velocities, either geometry could be suitable without a significant penalty in pressure drop.

The Liquid-to-Gas (L/G) ratio has been investigated by several authors as discussed before because it i) impacts the efficiency of the scrubber in capturing particles from the gas stream, ii) influences the mass transfer process between the gas and the liquid and iii) plays a role in determining the pressure drop across the venturi scrubber. Effects of L/G ratio on the pressure drop in both types of scrubbers for various water flow rates are depicted in Fig. 13. It is observed that, for both types of scrubbers, the pressure drop increases with the L/G ratio, and for the same flow rates, the circular scrubber tends to have a slightly higher pressure drop than the square scrubber. Regardless of the type of scrubber, higher water flow rates result in higher pressure drops.

The relationship between the Liquid/to-Gas (L/G) ratio and pressure drop for circular and square cross-sectional wet venturi scrubbers at various gas inlet velocities is presented in Fig. 14. The pressure drop increases with increasing the L/G ratio and gas inlet velocity for both types of scrubbers. Higher gas inlet velocities result in higher pressure drops for both designs, as reported for circular venturi scrubbers by [12]. This trend is consistent across all L/G ratios.

At all L/G ratios, higher gas inlet velocities result in substantially larger pressure drops compared to lower velocities, indicating the dominant contribution of gas-phase kinetic energy to overall hydraulic losses. For a given gas velocity, the circular scrubber exhibits higher pressure drops than the square cross-sectional one across the entire L/G range except at 10 m/s. The influence of the L/G ratio becomes more pronounced at elevated gas velocities, while at low gas velocities, the pressure drop remains relatively small and weakly sensitive to the L/G ratio for both geometries.

3.2.3 Collection efficiency

The collecting efficiency, which is defined as the ratio of the trapped water droplets at the walls to the injected droplets from the nozzle inlets of both designs, was also taken into consideration. At the wall, the droplets are removed, but their current mass and energies are imparted to the continuous (gas) phase. However, many models were proposed for the calculation of the performance of a venturi scrubber in the literature, as reported extensively by [34]. The influence of the scrubber geometry on the collection efficiency for various water rates and air flow velocities is shown in

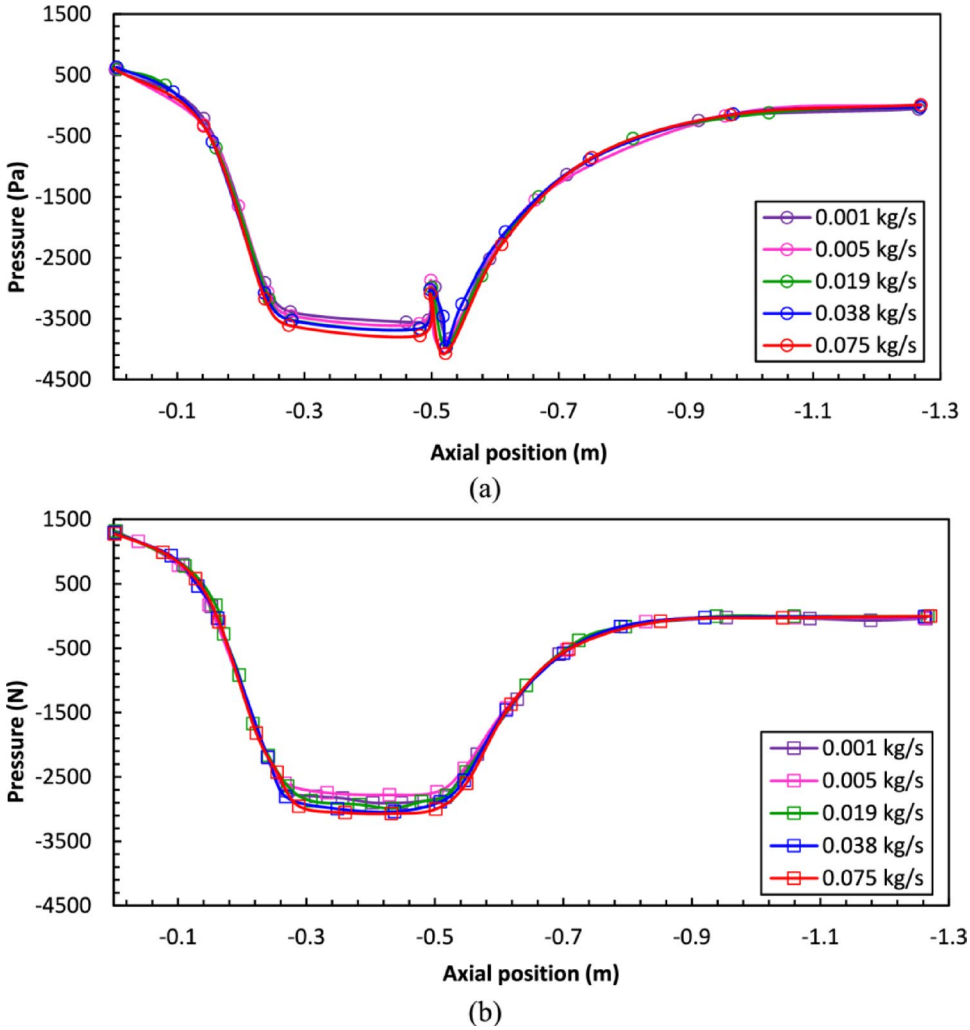

Fig. 11 Pressure change along the **a** circular and **b** square scrubber for various water mass flow rates, $V_g = 20$ m/s

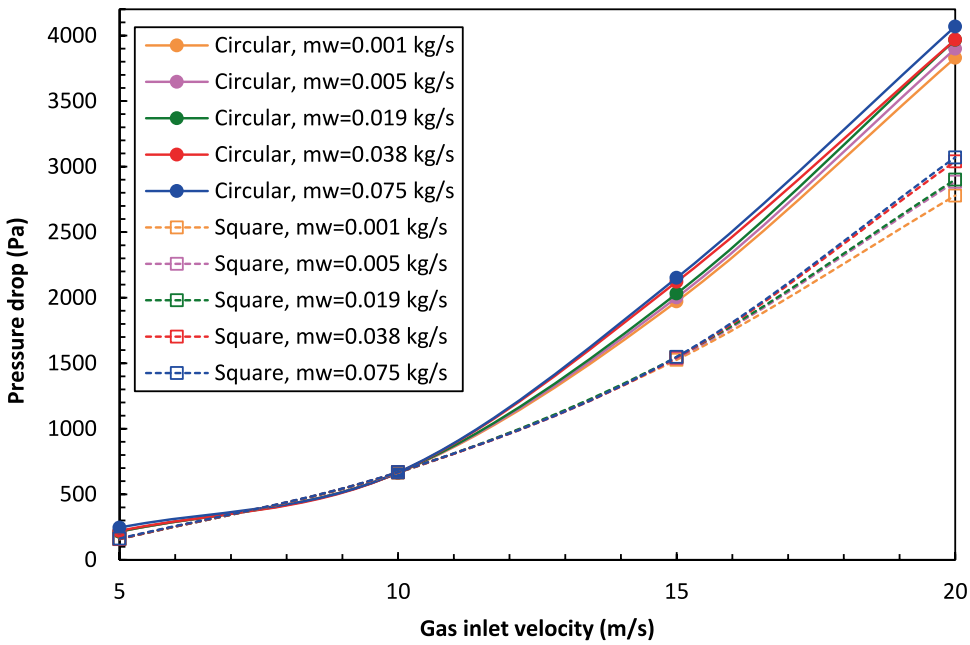

Fig. 12 Pressure drop variation with the gas inlet velocity and water flow rate in the circular and square venturies

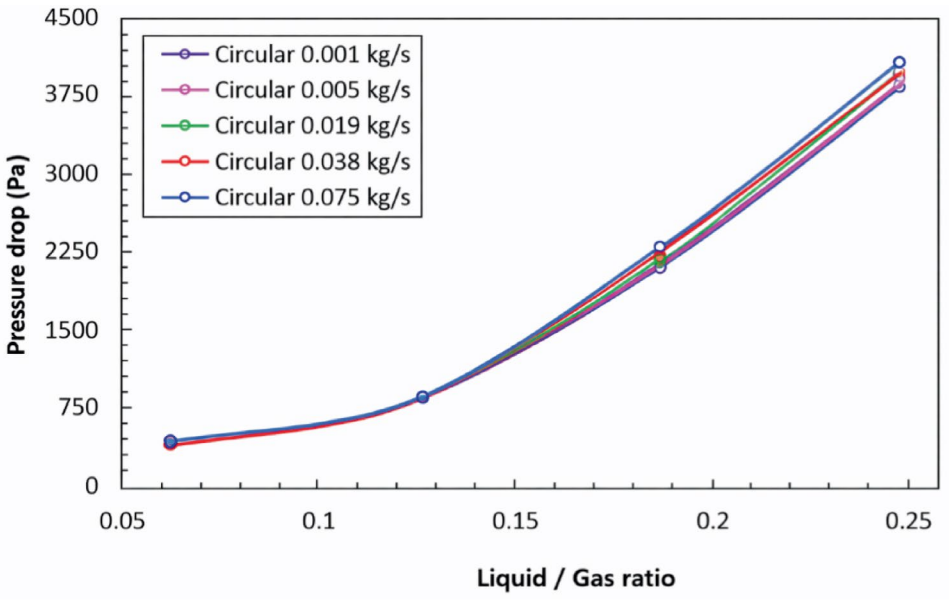

(a)

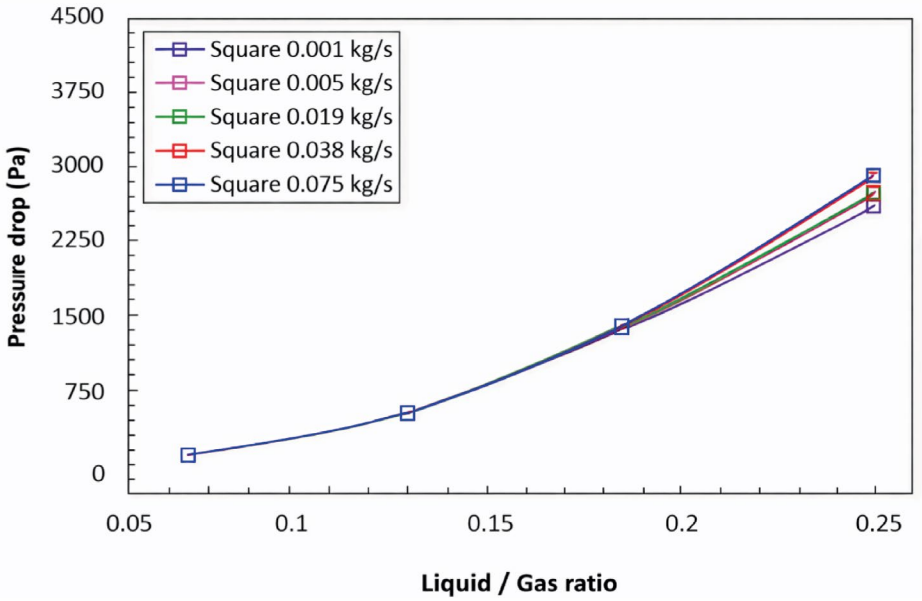

(b)

Fig. 13 Effect of Liquid/Gas ratio on the pressure drop in **a** circular and **b** square scrubber

Fig. 15. The overview of the plots clearly shows that the square scrubbers generally have higher initial collection efficiency compared to circular scrubbers at the same gas inlet velocity and that both scrubbers show a similar pattern of efficiency decline with increasing water flow rates. This is likely because the square geometry creates areas of recirculation and turbulence. For both scrubber shapes, higher gas inlet velocity tends to result in lower collection efficiency. The decline in collection efficiency with increasing water flow rate is steeper for higher gas inlet velocities.

The change in collection efficiency with varying water flow rates is illustrated in Fig. 16**.** For the circular scrubber, it is observed that the highest efficiency is observed at the lowest water flow rate. There is a gradual decline in efficiency with increasing velocity. The overall efficiency is lower compared to the square scrubber. For the square scrubber, it is clear that the highest efficiency is also at the lowest water flow rate and remains stable across all velocities. The square scrubber maintains higher efficiency compared to the circular scrubber at corresponding water flow rates. The results suggest that the square scrubber generally performs better than the circular scrubber in terms of collection efficiency across different water flow rates and velocities. Additionally, both scrubbers show their highest efficiency at the lowest flow rate, with the square scrubber maintaining higher efficiency overall.

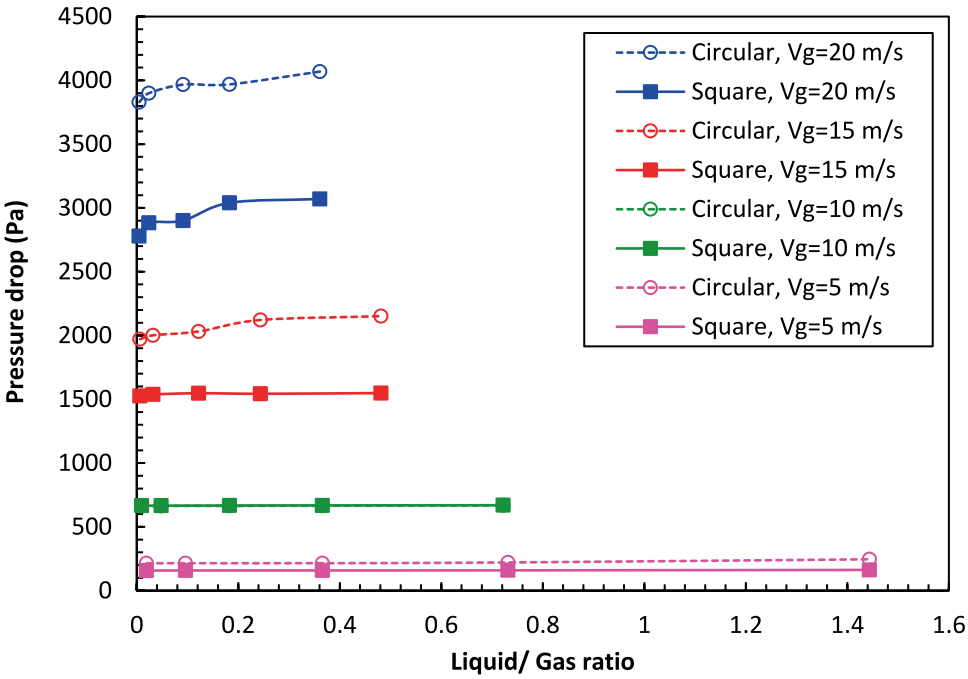

Fig. 14 Liquid-to-gas ratio on the pressure drop in circular and square cross-sectional scrubbers for various gas inlet velocities

4 Conclusion

The present study introduces a comprehensive investigation of the hydrodynamic performance of both circular and square cross-sectional wet venturi scrubbers having the same dimensions under the identical operating conditions using the Euler–Lagrange approach combined with the Discrete Phase Model. The credibility of the study is successfully presented for single and two-phase flow against both experimental and numerical data found in the related literature. Several paramount parameters in the design of scrubbers such as pressure drop, velocity distribution, liquid-to-gas ratio and collection efficiency, are investigated for various water flow rates and air inlet velocities. The single-phase flow analysis reveals that, at the same gas inlet velocity, almost identical velocity distribution is obtained for both geometries until the divergence section. Then, velocity is nearly constant along the square cross-sectional scrubber while it reduces gradually in the circular counterpart. For the specified inlet gas velocity, the pressure drop in the circular cross-sectional scrubber is higher than the square cross-sectional one. The double-phase flow investigations reveal that pressure distributions do not change considerably with the water changing flow rate. While the square scrubber induces a slightly lower pressure drop compared to its circular counterpart, it generates a more turbulent flow pattern due to its geometry, leading to a higher collection efficiency. Under the same operating conditions, the square scrubber can provide a higher collection efficiency, up to 96%, while the circular scrubber's efficiency is only 58%. Nevertheless, it is seen that increasing the water flow rate causes a notable reduction in collection efficiency, by 24% in the circular and 21% in the square cross-sectional scrubber. Therefore, it can be concluded that operational adjustments are necessary to maintain optimal performance at higher flow rates. The analyses on the effect of the liquid-to-gas (L/G) ratio on the pressure drop indicate that the pressure drop slightly increases with increasing L/G ratios, particularly at higher velocities in the circular scrubber; however, at lower velocities, the difference between the two scrubbers diminishes. In this context, it can be concluded that the square scrubber may be more efficient in applications requiring lower pressure drops and higher collecting efficiency, specifically at higher gas velocities and L/G ratios.

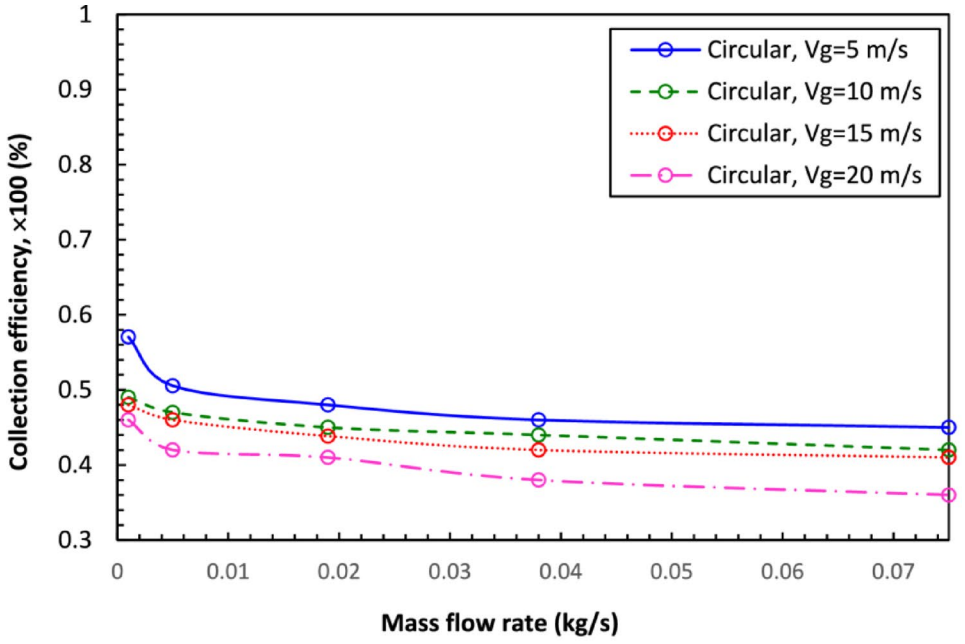

(a)

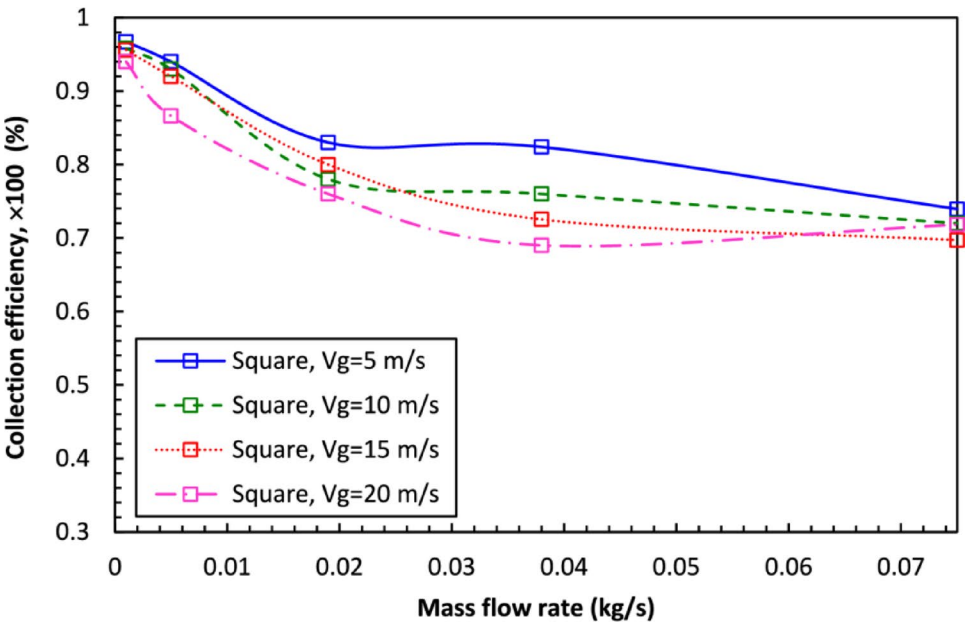

(b)

Fig. 15 Change of collection efficiency of the **a** circular and **b** square scrubber with gas inlet velocity

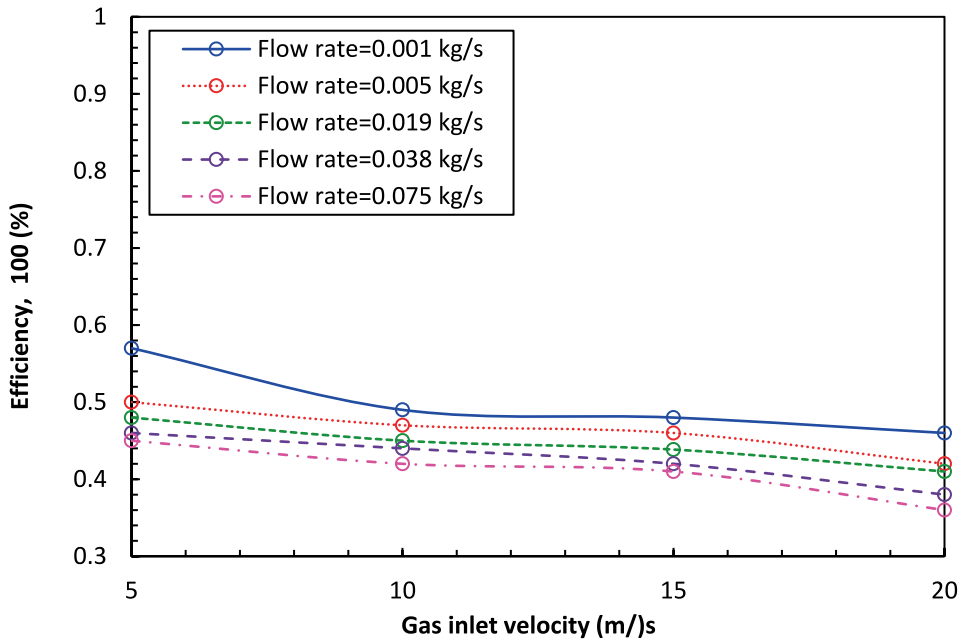

(a)

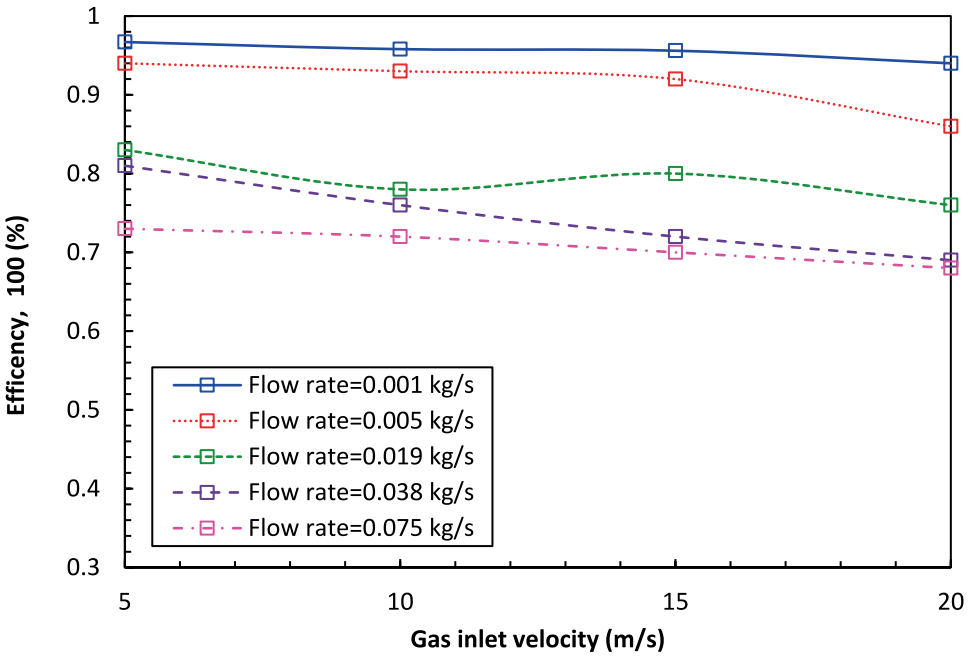

(b)

Fig. 16 Change of collection efficiency of the **a** circular and **b** square scrubber with various water flow rates

Funding Open access funding provided by the Scientific and Technological Research Council of Türkiye (TÜBİTAK).

Data availability The data that support the findings of this study are available within the article.

Declarations

Conflict of interest The authors declare that they have no known competing financial interests or personal relationships that could have appeared to influence the work reported in this paper.

Open Access This article is licensed under a Creative Commons Attribution 4.0 International License, which permits use, sharing, adaptation, distribution and reproduction in any medium or format, as long as you give appropriate credit to the original author(s) and the source, provide a link to the Creative Commons licence, and indicate if changes were made. The images or other third party material in this article are included in the article's Creative Commons licence, unless indicated otherwise in a credit line to the material. If material is not included in the article's Creative Commons licence and your intended use is not permitted by statutory regulation or exceeds the permitted use, you will need to obtain permission directly from the copyright

holder. To view a copy of this licence, visit http://creativecommons.org/licenses/by/4.0/.

References

1. Ahad J, Rizwan T, Farooq A, Waheed K, Ahmad M, Qureshi KR, Siddique W, Irfan N (2023) Study of hydrodynamics and iodine removal by self-priming venturi scrubber. Nucl Eng Technol 55(1):169–179. https://doi.org/10.1016/j.net.2022.09.005
2. Ahad J, Farooq A, Siddique W, Ahmed A, Ahmad M, Waheed K, Qureshi KR, Irfan N (2022) Influence of variation in converging section and orifice plane on the performance of venturi scrubber by using CFD. Prog Nucl Energy 151:104323. https://doi.org/10.1016/j.pnucene.2022.104323
3. Ahad J, Farooq A, Siddique W, Ahmed A, Ahmad M, Waheed K, Qureshi KR, Irfan N (2022) Influence of variation in converging section and orifice plane on the performance of Venturi scrubber by using CFD. Prog Nucl Energy 151:104323. https://doi.org/10.1016/j.pnucene.2022.10432
4. Ahmadvand F, Talaie MR (2010) CFD modeling of droplet dispersion in a venturi scrubber. Chem Eng J 160(2):423–431. https://doi.org/10.1016/j.cej.2010.03.030
5. Ahmed S, Mohsin H, Qureshi K, Shah A, Siddique W, Waheed K, Irfan N, Ahmad M, Farooq A (2018) Investigation of dust particle removal efficiency of self-priming venturi scrubber using computational fluid dynamics. Nucl Eng Technol 50(5):665–672. https://doi.org/10.1016/j.net.2018.01.016
6. Ali M, Yan C, Sun Z, Gu H, Mehboob K (2013) Dust particle removal efficiency of a venturi scrubber. Ann Nucl Energy 54:178–183. https://doi.org/10.1016/j.anucene.2012.11.005
7. Allen RWK, van Santen A (1996) Designing for pressure drop in venturi scrubbers: the importance of dry pressure drop. Chem Eng J Biochem Eng J 61(3):203–211. https://doi.org/10.1016/0923-0467(95)03044-1
8. Ananthanarayanan NV, Viswanathan S (1998) Estimating maximum removal efficiency in Venturi scrubbers. AIChE J 44(11):2549–2560. https://doi.org/10.1002/aic.690441122
9. ANSYS Inc (2023) ANSYS fluent user guide (Version 2023 R1). Canonsburg, PA: ANSYS, Inc
10. Attaullah Niazi MBK, Ahsan M, Ali M (2020) Computational fl uid dynamics simulation for theprediction of the venturi scrubber performance using fi nite volume method. Int J Comput Sci Math 11(4):38–346. https://doi.org/10.1504/IJCSM.2020.107601
11. Azzopardi BJ, Teixeira SFCF, Govan AH, Bott TR (1991) An improved model for pressure drop in venturi scrubbers. Trans Inst Chem Eng 69B:237
12. Azzopardi BJ (1992) Gas-liquid flows in cylindrical venturi scrubbers: boundary layer separation in the ditiser section. Chem Eng J 49(1):55–64. https://doi.org/10.1016/0300-9467(92)85025-5
13. Bal M, Meikap BC (2017) Prediction of hydrodynamic characteristics of a venturi scrubber by using CFD simulation. S Afr J Chem Eng 24:222–231. https://doi.org/10.1016/j.sajce.2017.10.006
14. Boll RH (1973) Particles collection and pressure drop in venturis scrubbers. Ind Eng Chem Fundam 12:40–50. https://doi.org/10.1021/i160045a008
15. Calvert S, Lundgren D, Mehta DS (1972) Venturi scrubber performance. J Air Pollut Control Assoc 22(7):529–532
16. Calvert S (1982) Scrubbing, air pollution, 3rd Edition, Vol. IV, Academic Press, New York, 1982
17. Costa MAM, Henrique PR, Gonçalves JAS, Coury JR (2004) Droplet size in a rectangular venturi scrubber. Braz J Chem Eng 21(02):335–343
18. Costa MAM, Ribeiro APRA, Tognetti ER, Aguiar ML, Gonçalves JAS, Coury JR (2005) Performance of a venturi scrubber in the removal of fine powder from a confined gas stream. Mater Res 8(2):177–179
19. Gonçalves JAS, Alonso DF, Costa MAM, Azzopardi BJ, Coury JR (2001) Evaluation of the models available for the prediction of pressure drop in venturiscrubbers. J Hazard Mater 81(1–2):123–140. https://doi.org/10.1016/S0304-3894(00)00336-8
20. Guerra VG, Bettega R, Gonçalves JAS, Coury JR (2012) Pressure drop and liquid distribution in a venturi scrubber, experimental data and CFD simulation. Ind Eng Chem Res 51(23):8049–8060. https://doi.org/10.1021/ie202871q
21. Guerra VG, Achiles AE, Bettega R (2017) Influence of droplet size distribution on liquid dispersion in a venturi scrubber: experimental measurements and CFD simulation. Ind Eng Chem Res 56(8):2177–2187. https://doi.org/10.1021/acs.iecr.6b03761
22. Haller H, Muschelknautz E, Schultz T (1989) Venturi scrubber calculation and optimization. Chem Eng Technol 12(1):88–195. https://doi.org/10.1002/ceat.270120125
23. Hesketh HE (1974) Atomization and cloud behaviour in wet scrubbers, Proceedings of the US–USSR, symposium on control fine particulate emissions, San Francisco, 15–18 January
24. Hollands KGT, Goel KC (1975) A general method for predicting pressure loss in venturi scrubbers. Ind Eng Chem Fundam 14(1):16–22
25. Jiang ZA, Huang YP (1995) Experimental study on a new wet dust collector. Saf Coal Mines 9:2–5
26. Khadra H, Kouider R, Tayeb NT, Al-Kassir A, Carrasco-Amador JP (2022) Numerical simulation of the cleaning performance of a Venturi scrubber. Energies. https://doi.org/10.3390/en15041531
27. Lee CH, Choi H, Jerng DW, Kim DE, Wongwises S, Ahn HS (2019) Experimental investigation of microbubble generation in the Venturi nozzle. Int J Heat Mass Transfer 136:1127–1138. https://doi.org/10.1016/j.ijheatmasstransfer.2019.03.040
28. Lehner M (1998) Aerosol separation efficiency of a Venturi scrubber working in self-priming mode. Aerosol Sci Technol 28:389–402. https://doi.org/10.1080/02786829808965533
29. Leith D, Cooper DW, Rudnick SN (1985) Venturi scrubbers: pressure drop and regain. Aerosol Sci Technol 4(2):239–243. https://doi.org/10.1080/02786828508959052
30. Maliqaj G (2016) Numerical simulation of flow in the wet scrubber for desulfurization, Diploma thesis, Technical University of Liberec, Czechia.
31. Mohebbi A, Taheri M, Fathikaljahi J, Talaie M (2003) Simulation of an orifice scrubber performance based on Eulerian/Lagrangian method. J Hazard Mater 100(13):13–25. https://doi.org/10.1016/S0304-3894(03)00066-9
32. Oruc M, Salih M, Yayla S et al (2024) Numerical studies on the oil-water mixture separation by corrugated plates with hooks and holes in various shapes and configurations. Arab J Sci Eng. https://doi.org/10.1007/s13369-024-09560-y
33. Pak SI, Chang KS (2006) Performance estimation of a Venturi scrubber using a computational model for capturing dust particles with liquid spray. J Hazardous Mater 138(3):560–573. https://doi.org/10.1016/j.jhazmat.2006.05.105
34. Rudnick SN, Koehler J, Martin KP, Leith D, Cooper DW (1986) Particle collection efficiency in a Venturi scrubber: comparison of experiments with theory. Environ Sci Technol 20(3):237–242. https://doi.org/10.1021/es00145a002. (**1;**)
35. Safdar I, Khan A, Ali M, Mushtaq A (2017) Numerical simulation of particulate removal efficiency in venturi scrubber, 13th international conference on emerging technologies (ICET), Islamabad, Pakistan, 2017, pp. 1–6, https://doi.org/10.1109/ICET.2017.8281727
36. Semrau KT, Marynowski CW, Lunde KE, Lapple CE (1958) Influence of power input on efficiency of dust scrubbers. Ind Eng Chem 50(11):1615–1620

37. Sharifi A, Mohebbi A (2014) A combined CFD modeling with population balance equation to predict pressure drop in Venturi scrubbers. Res Chem Intermed 40:1021–1042. https://doi.org/10.1007/s11164-013-1018-2
38. Shukla PK, Mishra R, Tewari RP (2023) Analysis of rotary ventricular assist devices using CFD technique—a review. Proc Inst Mech Eng E J Process Mech Eng 237(3):1036–1063. https://doi.org/10.1177/09544089221128366
39. Silva AM, Teixeira JCF, Teixeira SFCF (2009) Experiments in a large-scale venturi scrubber: Part I: pressure drop. Chem Eng Process Process Intensif 48(1):59–67. https://doi.org/10.1016/j.cep.2008.02.001
40. Silva AM (2008) Numerical and Experimental study of venturi scrubbers, Ph.D thesis, University of Minho, Portugal
41. Sjostrand E (2023) Desulphurisation of cement flue gases, Degree project in chemical engineering, Stockholm, Sweden
42. Sunday N, Settar A, Chetehouna K, Gascoin N (2021) Studying the effect of turbulence models on flow pattern and pressure drop for a two-phase hydrocarbon flow in horizontal pipelines using Openfoam. AIP Conference Proceedings of ICNAAM 2021, Sep 2021, Rhodes, Greece. ffhal-03869310f
43. Talaie MR, Mokhtarian N, Talaei A, Karimikhosroabadi M,Sadeghi F (2009) Experimental and theoretical investigation of droplet dispersion in venturi scrubbers with axialliquid injection. Chem Eng Technol 32(5):798–804. https://doi.org/10.1002/ceat.200800327
44. Tan Z, Zeng X, Shao S, Chen J, Wang H (2022) Scrubber installation and green fuel for inland river ships with non-identical streamflow. Transp Res E Logist Transp Rev 161:102677. https://doi.org/10.1016/j.tre.2022.102677
45. Tran TA (2017) Research of the scrubber systems to clean marine diesel engine exhaust gases on ships. J Marine Sci Res Develop 7(6):1–9. https://doi.org/10.4172/2155-9910.1000243
46. Turkoglu F, Bayraktar S (2025) Effects of different turbulence models on hydrodynamic performance of circular and square section scrubbers (in Turkish). Int J Adv Eng Pure Sci 37(1):8–18. https://doi.org/10.7240/jeps.1590292
47. Turkoglu F, Bayraktar S (2023) Effects of the nozzle location on hydrodynamic properties of a venturi-type scrubber, The 3rd International conference on innovative academic studies, September 26–28, Konya, Turkey
48. Viswanathan S, Gnyp AW, St. Pierre CC (1997) Estimating film flow in a Venturi scrubber. Part Sci Technol 15:65–76. https://doi.org/10.1080/02726359708906710
49. Xu Y, Gao L, Zhao Y, Wang H (2014) Wet gas overreading characteristics of a long-throat Venturi at high pressure based on CFD. Flow Meas Instrum 40:247–255. https://doi.org/10.1016/j.flowmeasinst.2014.09.004
50. Yan Z (2023) Development in comprehensive CFD simulation of fire and explosion. J Saf Sci Resil 4(2):203–219. https://doi.org/10.1016/j.jnlssr.2022.12.003
51. Yang X, Xi T, Qin Y, Zhang H, Wang Y (2024) Computational fluid dynamics–discrete phase method simulations in process engineering: a review of recent progress. Appl Sci Basel 14:3856. https://doi.org/10.3390/app14093856
52. Yung SC, Barbarika HF, Calvert S (1977) Pressure loss in Venturi scrubbers. J Air Pollut Control Assoc 27(4):348–351
53. Zhou Y, Sun Z, Gu H, Miao Z (2015) Experimental research on aerosols collection performance of selfpriming venturi scrubber in FCVS. Prog Nucl Energy 85:771–777. https://doi.org/10.1016/j.pnucene.2015.09.009

Publisher's Note Springer Nature remains neutral with regard to jurisdictional claims in published maps and institutional affiliations.